

CELLO FFT IMPEDANCE ANALYSIS AS A ROUTINE TOOL FOR IDENTIFYING VARIOUS DEFECT TYPES ON CRYSTALLINE SILICON SOLAR CELLS

J. Carstensen, A. Schütt, and H. Föll

Institute for Materials Science, Faculty of Engineering, Christian-Albrechts-University of Kiel,
Kaiserstr. 2, 24143 Kiel, Germany, email: jc@tf.uni-kiel.de, Phone: (+49) 431 880 6181, Fax: (+49) 431 880 6178

ABSTRACT: Decisive improvements of the CELLO hardware now allow FFT impedance analysis on large area solar cells of various types. Measuring the frequency response of the short circuit current for several frequencies simultaneously reduces the measurement time drastically. Fitting of the data to the complete impedance model of a solar cell allows to determine local solar cell properties like lifetime τ , back side recombination velocity S_b , and the time constant related to the $R_{ser} C_D$. Comparison with standard CELLO maps allows to quantify the efficiency losses related to the identified defect types.

Keywords: characterization, defects, lifetime

1 INTRODUCTION

The standard CELLO (solar CELI LOcal characterization) technique analyzes the current and voltage responses of a globally illuminated solar cell to local illumination with an intensity modulated LASER beam [1] at various points along the iv-curve. Using low frequencies leading to a negligible phase shift in the response data allows a rather straightforward interpretation of the measurements. In a different approach, called "FFT impedance analysis" and dubbed "CELLOplus", a wide range of modulation frequencies is chosen [2]; taking into account the full dynamics of the solar cell this allows to extract nearly all local transport and recombination parameters. The biggest obstacle for applying this mode to large solar cells is the capacitance of the cells proportional to their size. In combination with the ohmic losses in the grid and the wiring of the solar cell the corresponding large RC time constant leads to a resonant behavior of the measurement system that can principally not be overcome [3]. Substantial progress in optimizing the hardware minimizes this effect to tolerable levels and an impedance analysis of large solar cells of various types is now routine. Since several frequencies can be simultaneously applied for modulating the LASER intensity, the measurement time can be reduced significantly [2].

2 MODELLING OF SOLAR CELL IMPEDANCE

Fig. 1 shows the simplest model for the solar cell impedance that contains transport and recombination properties in the bulk and at back surface of the cell (represented by I_{ph}). The resistance R_D and the capacitance C_D represent the pn-junction diode. At short circuit conditions $R_D = \infty$ can safely be assumed. A serial resistance R_{ser} represents the grid and the backside metallization. The impedance of this electrical network representing the solar cell is

$$Z_{RC} = \frac{1}{1 + i\omega R_{ser} C_D} \quad (1)$$

with a phase shift

$$\varphi_{RC} \approx \tan \varphi_{RC} = \omega R_{ser} C_D \quad (2)$$

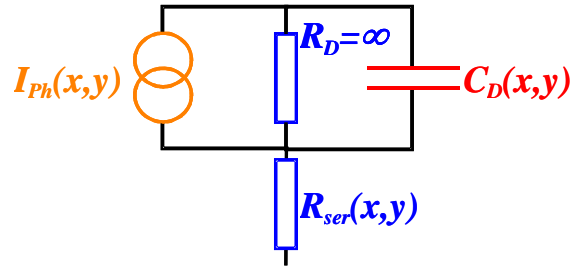


Figure 1: Model for local and global solar cell impedance at short circuit condition.

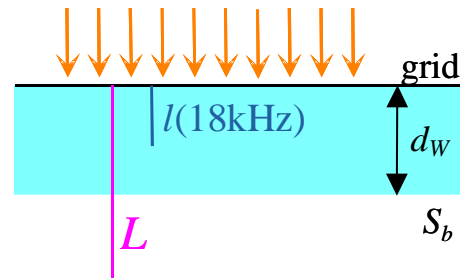


Figure 2: Typical length scales on solar cells.

The photo current is defined by generation, diffusion, and recombination in the bulk and at the interface at the backside. Details of the impedance related to these processes can be found in [3, 4]. The frequency dependence can be easily described by transforming the diffusion length

$$L := \sqrt{D\tau}, \quad (3)$$

where D is the diffusion coefficient and τ the lifetime, into an effective diffusion length \tilde{L} which is defined by

$$\frac{1}{\tilde{L}} = \frac{1}{\sqrt{D}} \sqrt{\frac{1}{\tau} + i\omega}. \quad (4)$$

The frequency dependent impedance for generation, diffusion and recombination of minority carriers is then described by the impedance (cf. [4])

$$Z_{Si}(\tau, D, S_B, R, \alpha, d_w, \omega) = qF(1 - R_{eff}) \frac{1 - \frac{1}{\tilde{L}\alpha} \left(1 - \frac{S_B}{D\alpha}\right) - \tanh\left(\frac{d_w}{\tilde{L}}\right) \left(\left(\frac{1}{\tilde{L}\alpha}\right)^2 - \frac{S_B}{D\alpha}\right)}{1 - \left(\frac{1}{\tilde{L}\alpha}\right)^2 - \frac{1}{\tilde{L}\alpha} - \tanh\left(\frac{d_w}{\tilde{L}}\right) \frac{S_B}{D\alpha}} \quad (5)$$

Here S_B is the surface recombination at the back side, F is the over all photon flux of the LASER beam, R_{eff} is the reflectivity, α is the absorption coefficient, and d_w is the thickness of the solar cell.

At low frequencies $\tilde{L} \rightarrow L$. For higher frequencies $\tau^{-1} \rightarrow 0$, thus a second length scale l dominates, given by

$$\frac{1}{l} := \frac{1}{\sqrt{D}} \sqrt{i\omega} \quad (6)$$

Fig. 2 displays the relations for solar cells with a thickness $d_w = 300 \mu\text{m}$ and a diffusion length $L = 500 \mu\text{m}$. At low modulation frequencies the short circuit current will be sensitive to S_b because $L > d_w$. Taking a diffusion coefficient $D = 23 \text{ cm}^2 / \text{s}$ at 18 kHz we find an already quite small $l \approx 140 \mu\text{m}$, i.e. no information of the recombination at the backside of the wafer can reach the front side where the photo current is collected. So the short circuit current induced by a Laser modulation frequency of 18 kHz will not be sensitive to S_b .

Eqs. (1) - (4) already allow for a qualitative understanding of the impedance data presented in this paper. For most solar cells the phase shift φ_{Si} calculated from Eq. (5) is much smaller than φ_{RC} described by Eq. (2). This fact and the linear relation between φ_{RC} and the applied frequency allows to eliminate completely the influence from grid and pn junction capacitance from the phase shift maps by calculating the frequency corrected difference $\Delta\gamma$ of phase shift maps measured at different frequencies, i.e.

$$\Delta\varphi = \varphi(\omega_1) - \varphi(\omega_2) \frac{\omega_1}{\omega_2} \quad (7)$$

The resulting CELLOplus map only contains information about τ , D , and S_B which allows for a better qualitative understanding of local recombination processes, but it does not allow to get quantitative data. Only a complete least square fit of the measured frequency dependent data to the full impedance model allows to extract all parameters locally as will be demonstrated in the following.

3 EXPERIMENTAL RESULTS AND DISCUSSION

In this paper we present short circuit current CELLOplus impedance results as well as standard CELLO maps for a 12.5 cm x 12.5 cm mc-Si solar cell with a thickness of 300 μm . **Fig. 3a)** shows the amplitude map $dI_{sc}(3.5\text{kHz})$. It shows a large range in the amplitude values; around the main bus bars significantly smaller current amplitudes are found. Since this is not easily visible in the full maps a zoom of a part around the upper right bus bar is shown in the inset in all maps. Some grains show extremely large numbers while especially the currents in the upper left part of the cell are smaller. The

corresponding phase shift map in **Fig. 3b)** shows much less lateral variation. The grain boundaries as well as the areas around the main bus bars have very small phase shifts. Increasing the frequency to 15kHz new features become visible in the phase shift map in **Fig. 3c)**. Especially near the lower and left edge of the cell, regions with increased phase shifts show up. According to the discussion leading to Eq. (7) one can expect these structures to be induced by a larger value of the RC time constant. To check this, the frequency corrected phase shift difference (cf. Eq. (7)) is plotted in **Fig. 3d)**. Here the dark areas slightly visible in **Fig 3b)** and clearly visible in **Fig 3c)** become completely invisible. The map in **Fig. 3d)** only contains information about diffusion and recombination in the bulk and at the interface at the backside. All grain boundaries as well as the already mentioned regions around the main bus bars show smaller numbers in **Fig. 3d)**. With some experience in impedance analysis of solar cells one might confidentially guess that the amplitude losses around the main bus bars are related to a missing back surface field (BSF), but neither of the maps shown allows to obtain numbers for the bulk lifetime or the surface recombination velocity.

A fit of the complete model to all CELLOplus maps (here 3 amplitude and 3 phase shift maps) is needed to extract the full information. **Fig. 4** shows the main results. In **Fig. 4a)** the numbers for $qF(1 - R_{eff})$ are plotted, i.e. the local photon flux into the solar cell, mainly representing reflectivity losses. Comparing **Fig. 3a)** and **Fig. 4a)** shows that most of the dynamics in the amplitude of the photocurrent is simply related to differences in the reflectivity. This example has been chosen to demonstrate that the impedance analysis can compensate for these differences without any direct measurement of the reflectivity. On the other hand it is also obvious that the current losses around the main bus bars are not related to increased reflectivity; these areas show increased recombination losses, indeed. **Fig. 4b)** shows the lifetime map, **Fig 4c)** the map of S_B both maps are quantitative. As expected, the recombination losses around the main bus bars result from a missing BSF leading to large values of S_B . Just a very small reduction of the bulk life time is found in these areas according to the fit. At this time it is not clear if this is a real physical effect or a small fitting artifact.

Lack of space prevents a detailed discussion of measurement errors and their consequences on the resulting fitting parameters. Quite obviously the results are at least qualitatively correct, and more involved arguments show that the numbers are very likely correct within a factor less than 2. The results would become significantly more robust if impedance data would be obtained with two LASERs having different penetration depths, i.e. by coupling impedance analysis and spectral response analysis. This approach will be tested in the near future.

As expected, the map structures that were already identified as RC related by just checking the frequency dependence of the phase shift, do show up in the RC map **Fig. 4d)**. It can be concluded from the peculiar geometry that the observed increased RC time constant is most likely due to a locally bad contact resistance between grid fingers and the emitter. In addition, all edges show increased serial resistances just because the backside metalization as well as the front grid does not reach these areas.

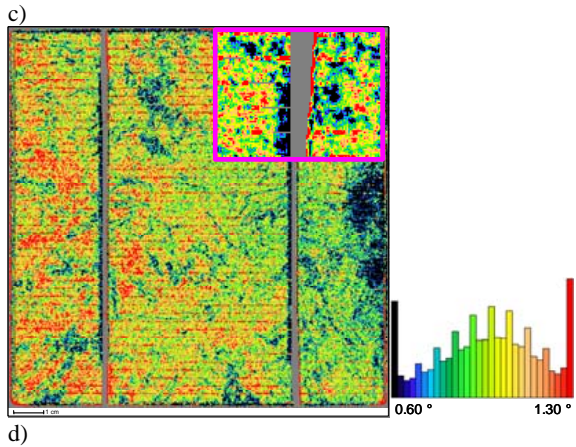
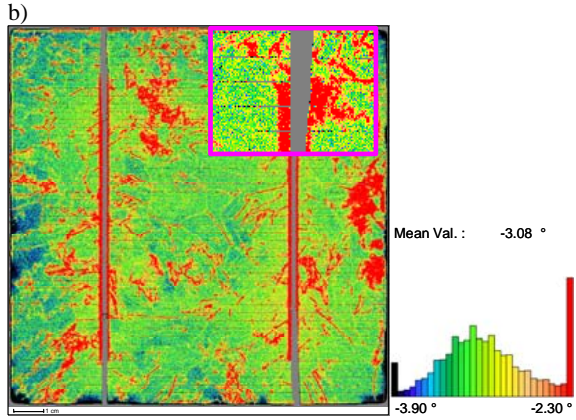
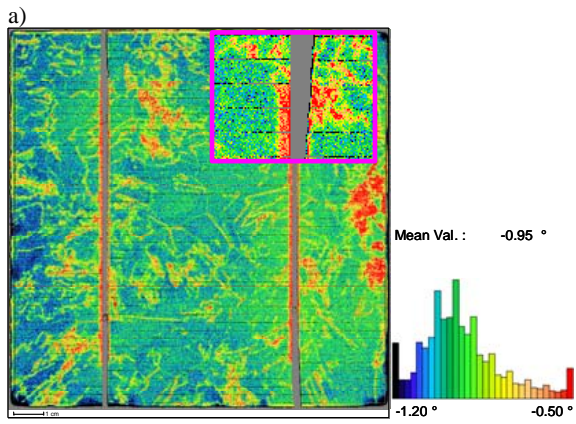
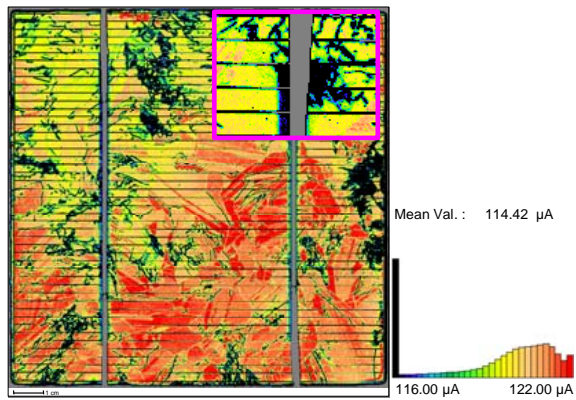


Figure 3: CELLOplus measurement results for short circuit currents. a) Amplitude map at 3.5 kHz. b) Phase shift map at 3.5 kHz. c) Phase shift map at 15 kHz. d) Frequency corrected difference of the phase shift (map b) and map c) using Eq. (7).

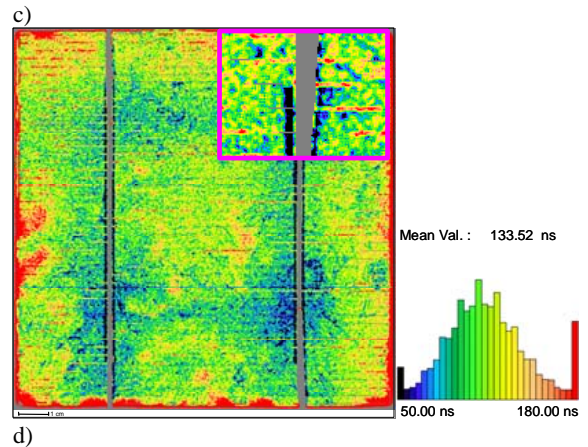
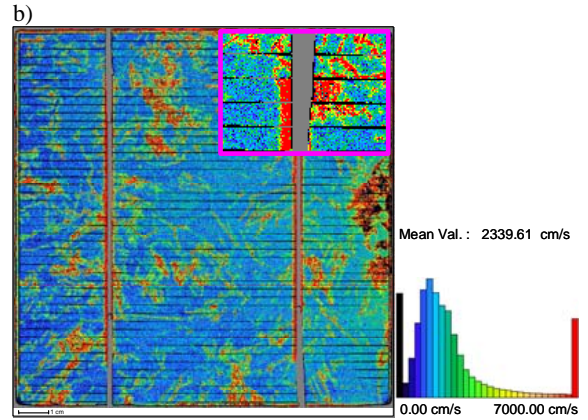
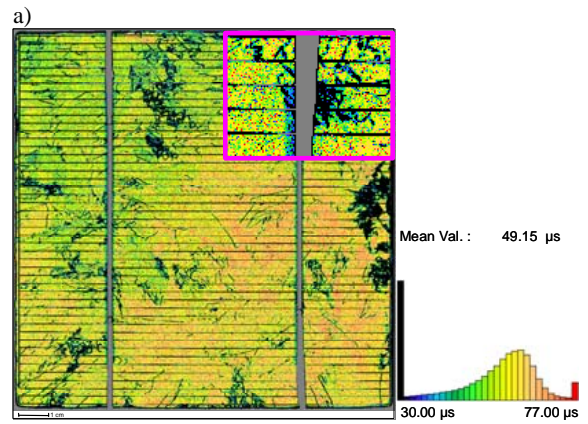
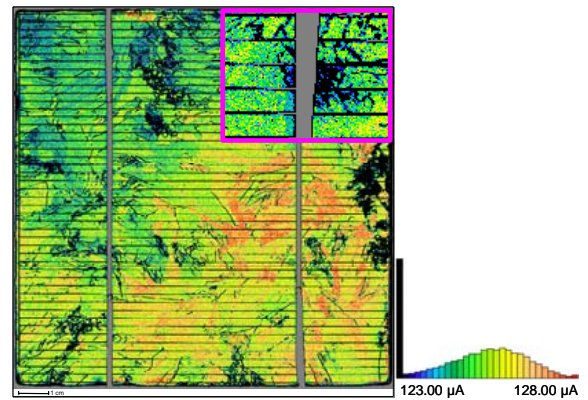


Figure 4: Parameter maps resulting from fitting CELLOplus measurements to the complete solar cell impedance. a) Map of $qF(1 - R_{eff})$ containing the reflectivity losses. b) Lifetime τ map. c) Backside surface recombination velocity S_b map; d) $R_{ser} C_D$ map.

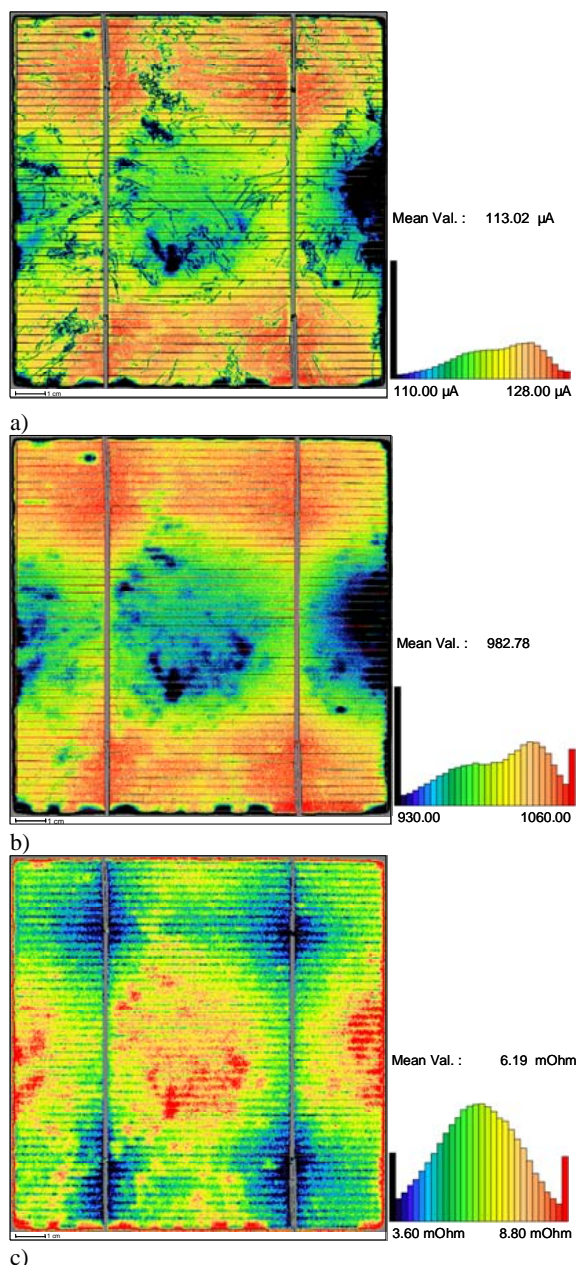


Figure 5: Results from standard CELLO maps. a) Amplitude of the current at the working point of the solar cell. b) Ratio between the current at the working point (**Fig. 5 a**) and the current under short circuit condition (**Fig. 3 a**). c) Standard CELLO R_{ser} map calculated from the open circuit voltage map.

Although **Fig. 4** summarizes nearly all local parameters relevant for the solar cell efficiency it would need complicated simulations to answer the most important question: "What is the dominant defect structure limiting the efficiency at the working point of the solar cell?" This question, however, can be directly answered with standard CELLO measurements, e.g. by measuring the photo current at the working point of the solar cell; the result is shown in **Fig. 5a**). The smallest currents are found at the right edge of the solar cell around a large area with a high dislocation density. Calculating the ratio between the current at the working point and the short circuit currents shown in **Fig. 5b**), it becomes obvious that the losses in this area are much stronger than just the losses in the

short circuit current. These losses are induced by a lateral current flow from good areas of the solar cell into the bad area. These losses are so severe because the structure is located at the edge of the cell far away from the main bus bars. The ohmic losses are so large just because the distance is large and the current is large, not because the grid resistance is large in this area. Of course, the areas with contact resistance problems show up in **Fig. 5a**) and **5b**) as well but their over-all effect is small compared to that induced by the lateral current flow. Ohmic losses lead to a reduced filling factor. Just placing this bad area near to a main bus bar would significantly reduce the losses in the filling factor.

Fig. 5c) shows the standard CELLO serial resistance map, extracted mainly from voltage measurements at open circuit condition. In this map the bad area is visible as well but is no more prominent than the areas with large contact resistance. Comparing **Fig. 5c**) with the RC map in **Fig. 4d**) a quite good agreement is found. This indicates that the capacitance of the pn-junction is quite constant across the solar cell. The differences between **Fig. 4d**) (short circuit), **Fig. 5b**) (working point), and **Fig. 5c**) (open circuit) are not measurement artifacts but a direct consequence of the (along the iv-curve) strongly changing diode resistance on the network of the distributed serial resistance as discussed in more detail in [5].

4 SUMMARY

Significantly improving the CELLO hardware now allows to analyze a large variety of solar cells by FFT impedance analysis. The resulting CELLOplus technique is a fast and powerful tool to characterize in detail local cell properties like τ , S_b , and R_{ser} , C_D . In combination with a standard CELLO analysis the impact of the identified local defect types on the solar cell efficiency can be analyzed.

5 ACKNOWLEDGMENTS

This work has been supported by the German network project "Netz Diagnostik" and by DFG grant FO 258/11-1.

6 REFERENCES

- [1] J. Carstensen, G. Popkirov, J. Bahr, and H. Föll, *Solar Energy Materials & Solar Cells* **76**, 599 (2003).
- [2] J. Carstensen, A. Schütt, and H. Föll, in *Proceedings of the 23rd European Photovoltaic Solar Energy Conference*, 1AO.6.1, Valencia (2008).
- [3] A. Schütt, S. Keipert, J. Carstensen, and H. Föll, in *Proceedings of the 22nd European Photovoltaic Solar Energy Conference*, 1CV.1.35, Milan (2007).
- [4] J. Carstensen, E. Foca, S. Keipert, H. Föll, M. Leisner, and A. Cojocaru, *Phys. Stat. Sol. (a)* **205(11)**, 2485 (2008).
- [5] J. Carstensen, A. Abdollahinia, A. Schütt, and H. Föll, in *Proceedings of the 24th European Photovoltaic Solar Energy Conference*, 1CV.4.33, Hamburg (2009).